Classification of Alzheimer's Disease from MRI Using Sulcal Morphology

Simon Kragh Andersen, Christian Elmholt Jakobsen, Claus Hougaard Pedersen, Anders Munk Rasmussen, Maciej Plocharski(✉), and Lasse Riis Østergaard

Department of Health Science and Technology, Aalborg University, Aalborg, Denmark
mpl@hst.aau.dk

Abstract. Alzheimer's disease (AD), an age-related progressive neurodegenerative disorder, is the most common cause of dementia. It is characterised by abnormal neuroanatomical changes in the brain, some of which can be difficult to distinguish from the alterations caused by normal aging. Sulcal morphology is affected by AD atrophy, indicates significant differences between cognitively normal (CN) and AD subjects, and proves to be a potential AD biomarker. 210 subjects (100 CN, 110 AD) were acquired from the ADNI database. 120 sulci were extracted per subject using BrainVISA sulcal identification pipeline. Mean curvature, surface area and volume were calculated for each sulcus, parameterized by a 3D mesh, and used as AD/CN classification features. 184 subjects were correctly classified (AD=98, CN=86), producing an accuracy of 88%, sensitivity of 89%, specificity of 86%, based on 33 features. Results indicate that sulcal morphology, when based on specific features, could be a valuable AD biomarker.

Keywords: AD · MRI · Sulcal morphology · Classification · Support vector machine · BrainVISA

1 Introduction

Dementia is a descriptive term indicating an observable decline in cognitive abilities. It is estimated that 35.6 million people were living with dementia in 2010, and this number is expected to almost double every 20 years as a result of the worldwide ageing population [1]. Alzheimer's disease (AD) is the most frequent neurodegenerative disease, the most common cause of dementia, and

Data used in preparation of this article were obtained from the Alzheimer's Disease Neuroimaging Initiative (ADNI) database (adni.loni.usc.edu). As such, the investigators within the ADNI contributed to the design and implementation of ADNI and/or provided data but did not participate in analysis or writing of this report. A complete listing of ADNI investigators can be found at: http://adni.loni.usc.edu/wp-content/uploads/how_to_apply/ADNI_Acknowledgement_List.pdf.

R.R. Paulsen and K.S. Pedersen (Eds.): SCIA 2015, LNCS 9127, pp. 103–113, 2015.
DOI: 10.1007/978-3-319-19665-7_9

is usually diagnosed in people over 65 years of age, but the early-onset AD can occur much earlier [2]. AD is an irreversible and progressive disorder, estimated to affect 60-65% of dementia patients [3]. By 2050 the expected prevalence of AD will have increased to 106.8 millions, from 30 millions in 2010 [4]. AD projection models suggest that primary prevention may successfully delay the onset of AD and as a result reduce the future prevalence of the disease.

Human brain morphology, the study of its form and shape, is considered a potential biomarker for diagnosis and prognosis of neurological diseases. Cortical thickness, surface area and its mean curvature, sulcal depth and width, have been applied to distinguish AD from CN [5,6]. Sulci are important macroscopic surface landmarks of the cerebral cortex (illustrated on Figure 1) which allow distinguishing between different functional areas of the brain. Their morphology has recently been utilized as means of investigating the structural brain changes, supplementing or replacing the measurements of cortical thickness, or approaches involving voxel-based methods. Sulcal surface and length as potential biomarkers have been investigated for Autism Spectrum Disorder [7], and they are also speculated to be in correlation with morphological changes in the cortex in schizophrenia, where sulcal abnormalities in language-related areas may be the underlying cause of hallucinations [8]. The atrophic changes in the brain are reflected in a loss of gray matter [9] and believed to first affect the entorhinal cortex and the hippocampus [10]. Sulcal widening, depth, and overall cortex atrophy have been linked with the progression of AD. The AD-related brain atrophy results in narrowing of cerebral gyri and widening of sulci. The widening of cortical sulci has been measured as a neuroimaging marker of brain atrophy, either age- or disease-related [6,11]. It is correlated with cognitive functions in the elderly, i.e. poorer cognitive performance was associated with a wider sulcal span [12].

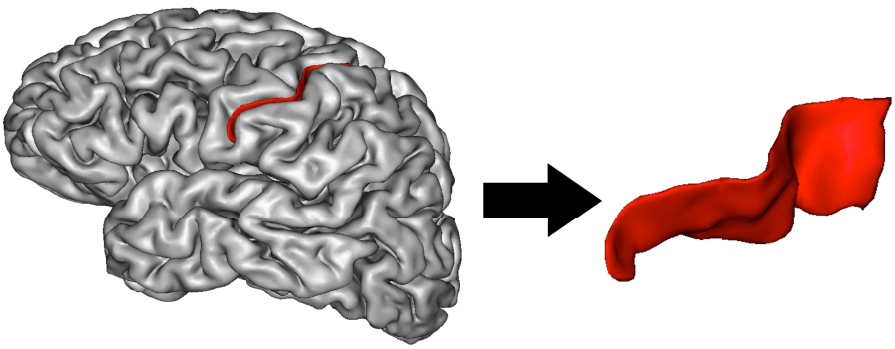

Fig. 1. Illustration of an extracted sulcal mesh by BrainVISA 4.4.0

Sulcal widening also showed the highest sensitivity in revealing differences between CN and AD [5]. Significant changes in sulcal depth have also been found

in normal aging [11], as well as in AD and mild cognitive impairment patients, where a relationship between sulcal shape and volumetric changes was investigated. Im et al., 2008 [5] found a significantly lower sulcal mean curvature in AD subjects than in normal controls, and a significant difference in sulcal depth between CN and AD. Another study used similarity maps to examine correlation of mean cortical thickness between region of interest (ROI) [13]. Multi-kernel support vector machine (SVM) was used to classify regional mean cortical thickness, hippocampal volume, regional cortical volumes and a combination of those in CN and AD subjects, with a classification accuracy of 92.35%, and an area of 0.9744 under the receiver operating characteristic (ROC) curve [13].

The purpose of this cross-sectional study was to investigate the sulcal morphology (mean curvature, surface area, volume) as biomarkers complementing the structural changes seen in MRI, which would provide a successful classification of AD. The contribution of this paper is that the pipeline successfully extracted, calculated and selected a feature combination of sulcal mean curvature, surface area, and volume for AD/CN classification using SVM, while earlier studies focused on individual analysis of sulcal length, depth, or width.

2 Methods

Data

Data used in this project was obtained from the ADNI database. The ADNI database was launched in 2003 by the National Institute on Aging (NIA), the National Institute of Biomedical Imaging and Bioengineering (NIBIB), the Food and Drug Administration (FDA), private pharmaceutical companies and nonprofit organizations, as a $60 million, 5-year public- private partnership. The primary goal of ADNI has been to test whether serial magnetic resonance imaging (MRI), positron emission tomography (PET), other biological markers, and clinical and neuropsychological assessment can be combined to measure the progression of mild cognitive impairment (MCI) and early AD. Determination of sensitive and specific markers of very early AD progression is intended to aid researchers and clinicians to develop new treatments and monitor their effectiveness, as well as lessen the time and cost of clinical trials.

210 1.5T pre-processed[1] T1-weighted magnetization-prepared rapid gradient echo (MP-RAGE) scans [CN (n=100), and AD (n=110)] were acquired from ADNI. The CN group was defined in the database as 'ADNI1 Screening', which consists of healthy controls, with no signs of depression, mild cognitive impairment nor dementia; while the AD group as 'ADNI1/GO Month 24', with AD subjects scanned 24 months after AD diagnosis. The criteria for CN were as follows: Mini-Mental State Examination (MMSE) score: 24-30, Clinical Dementia Rating (CDR) of 0, non–depressed, non MCI, and not demented. The criteria for AD were: MMSE score below 26, CDR of 0.5, and meet the National Institute of

[1] Image corrections are detailed at http://adni.loni.usc.edu/methods/mri-analysis/mri-pre-processing

Neurological and Communicative Disorders and Stroke-Alzheimer's Disease and Related Disorders Association criteria for probable AD. The demographics distribution for each group are represented in Table 1. T1-weighted MR scans were

Table 1. Demographics distribution of the subjects

Group	N (females)	Age ± sd	MMSE ± sd	CDR ± sd
AD	110 (52)	77.7±7.4	18.7±6.0	1.3±0.6
CN	100 (49)	75.8±5.3	29.1±1.1	0.0±0.0

processed in BrainVISA 4.4.0 Morphologist 2013 pipeline to extract sulci. Surface area, mean curvature, and volume were calculated. Exclusion criteria were applied to ensure the quality of the data. Figure 2 illustrates a simplified method pipeline. Selection of features was performed by means of forward selection and

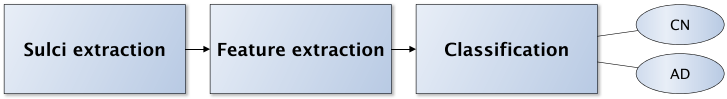

Fig. 2. A simplified pipeline for the AD/CN classification based on sulcal morphology

backward elimination in order to ensure that only the best selected features and feature combinations produce the highest classification results. Each iteration was investigated and evaluated on accuracy in a k-fold (k=10) cross-validation SVM classifier. BrainVISA 4.4.0 Morphologist 2013 pipeline was used to extract all sulci labeled in the BrainVISA Sulci Atlas v. 2011 (n=60) for both left and right hemisphere. The mesh files, converted from a NIfTI to a polygon file format (.ply), were analyzed in MATLAB R2014b. The meshes created by BrainVISA are converted from consist of two main components: a vector of three-dimensional vertices, connected by edges, and a vector of polygons, or mesh faces, where each polygon is defined by the three vertices it links. The overall surface of the mesh consists of the mesh faces.

Sulcal Extraction and Feature Selection

BrainVISA extracted 60 sulci from the left hemisphere and 60 from the right (120 sulci total) for each subject. The total number of all extracted sulci from 210 subjects was 25200. In principle, every sulcus had to be extracted twice from each subject: once from the left hemisphere, once from the right; and this extraction was attempted on all 210 subjects. However, BrainVISA was not able to successfully extract some of the sulci for a number of subjects, either due to lower quality MRI data, or due to an error in sulcal identification and

labeling. The following exclusion criterion was selected to avoid a situation where a certain sulcus would be extracted only in a small number. If the number of successful extractions for a given sulcus was below 95% of a total number of expected successful extractions from all 210 subjects, that specific sulcus was removed from the pooled data, both the left and right side. In this process, 48 sulci were removed. For each sulcus, three features were calculated: sulcal surface area, mean curvature, and volume, resulting a total of 216 features per subject: 108 from the left hemisphere and 108 from the right. Additionally, the ratios of the remaining features were created (n=108) (e.g. the ratio of a sulcus volume between the left and right hemisphere).

Surface Area: Heron's formula [14] was used to calculate the surface area of each triangle in the mesh. The total surface area was obtained by summing all thee triangles in the extracted sulcus.

Mean Curvature: The mean principal curvature of each sulcus was calculated by splitting the sulcus into parts consisting of one vertex, and the vertices connected via the face-matrix in two links or less. This part was then rotated into a normalized plane, and fitted to the function in Equation (1).

$$f(x, y) = \alpha_1 x^2 + \alpha_2 y^2 + \alpha_3 xy + \alpha_4 x + \alpha_5 y + \alpha_6 \tag{1}$$

α_1, α_2 and α_3 were used to create the Hessian matrix, from where the eigenvectors and eigenvalues were calculated. This was performed for every vertex in the sulcus. The mean of the eigenvalues was used as the mean curvature for the sulcus.

Volume: The volume for each sulcus in all subjects was calculated using Delaunay triangulation to split the sulcus into tetrahedrons. The volume for each tetrahedron was calculated by Equation (2). The total sulcal volume was defined as the total sum of all the tetrahedrons.

$$V = \frac{|(\boldsymbol{a} - \boldsymbol{d}) \cdot ((\boldsymbol{b} - \boldsymbol{d}) \times (\boldsymbol{c} - \boldsymbol{d}))|}{6} \tag{2}$$

$\boldsymbol{a}$, $\boldsymbol{b}$ and $\boldsymbol{c}$ are the coordinates for the base of the tetrahedron and $\boldsymbol{d}$ for the apex. All tetrahedrons with a circumsphere radius larger than a selected threshold (r=2) were removed.

The feature extraction and selection pipeline decreased the number of features from the initial 360 (surface area, mean curvature, and volume for 120 sulci per subject) to 324. The process of extracting and selecting features is illustrated on Figure 3. The next step involved selecting the features that best distinguish AD from CN by means of forward selection and backward elimination. During each iteration, 10-fold cross-validation was applied to evaluate the performance of the features, where the data was randomly partitioned into k=10 subgroups of equal size. A single subgroup was removed from the rest of the data, and

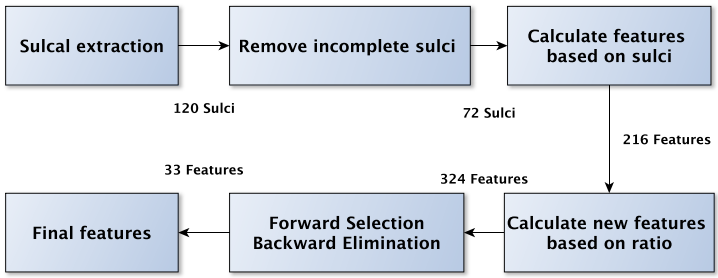

Fig. 3. Overview of the specific method pipeline, from feature extraction to obtaining final features

used as the validation data for testing the classification performance, while the remaining subgroups were used as training data. This cross-validation process was repeated k=10 times, where each subgroup was used exactly once. If the classification performance, based on a balancing index (below 0.40) [15] and the highest accuracy, performed better than the previous run, the feature was added to the feature set. This was repeated until adding additional features would not improve the outcome of the classifier. The highest classification accuracy was obtained with a set of 33 features.

Results

The two subject groups consisted of 110 AD and 100 CN subjects. The initial 324 features were used in a forward selection and backward elimination methods. A MATLAB SVM with a linear kernel was employed to evaluate the selected features with the following parameters: a standardized predictor matrix was used to train the classifier, and the prior probabilities for the two classes were uniform. Each iteration was evaluated based on a balancing index combined with accuracy in a 10-fold cross-validation SVM classifier. In Table 2 the sulci are sorted after feature type. The best feature combination consists of features related to surface area. Eleven features were based on sulcal surface area, and six were of the surface area ratio between the sulci in the left and the right hemisphere, resulting in a total of 17 surface area features. Eleven related to the sulcal curvature, out of which four were the ratio between the left and right hemisphere. Only five features were based on sulcal volume alone, not combined with the ratio between left and right hemisphere. The best classification result was obtained on 33 features, listed in Table 2, which shows in what order the features were selected and which were the most discriminating. 184 subjects were classified correctly (AD=98, CN=86), resulting with a sensitivity of 89%, specificity of 86% and accuracy of 88%. The receiver operating characteristic curve (ROC) and area under curve (AUC) were used to illustrate and evaluate the performance of the discrete classifier. The curve illustrates the true positive

Table 2. The 33 selected features, their means and standard deviations, sorted in what order they were selected and which were the most discriminating

Feat. no.	Sulcus:	Feature:	AD ± SD	CN ± SD
1	Superior temporal sulcus right	surface area	2520.75±581.07	2904.11±571.32
2	Calloso-marginal posterior fissure left	surface area	1144.14±381.26	1339.94±337.08
3	Posterior inferior temporal sulcus left	surface area	667.71±318.68	858.14±394.69
4	Calloso-marginal posterior fissure	surface area ratio	1.21±0.68	1.14±0.42
5	Central sulcus left	volume	1239.16±220.20	1215.34±207.26
6	Superior postcentral intraparietal sup. left	volume	471.79±202.23	540.54±233.63
7	Posterior intra-lingual sulcus left	volume	131.01±89.27	119.91±83.06
8	Olfactory sulcus right	surface area	513.06±132.77	566.39±152.23
9	Calloso-marginal posterior fissure right	curvature	0.13±0.04	0.11±0.05
10	Cuneal sulcus left	curvature	0.21±0.07	0.25±0.40
11	Rhinal sulcus right	surface area	290.27±225.70	292.93±186.07
12	Ascending ramus of the lateral fissure	surface area ratio	1.62±2.01	1.55±2.39
13	Posterior occipito-temporal lateral sulcus	curvature ratio	1.06±0.50	1.19±1.01
14	Posterior terminal ascending branch of superior temporal sulcus	curvature ratio	1.45±1.20	1.31±0.83
15	Anterior intralingual sulcus right	surface area	227.12±140.37	216.72±125.18
16	Rhinal sulcus right	curvature	0.22±0.13	0.21±0.07
17	Marginal frontal sulcus	surface area ratio	1.42±1.60	1.15±0.87
18	Olfactory sulcus right	volume	227.47±62.61	257.83±73.86
19	Anterior inferior temporal sulcus right	surface area	600.47±270.84	676.03±219.91
20	Central sulcus	surface area ratio	1.05±0.19	1.03±0.18
21	Internal frontal sulcus	surface area ratio	1.29±0.86	1.47±1.17
22	Polar frontal sulcus left	curvature	0.31±0.30	0.27±0.13
23	Posterior lateral fissure left	curvature	0.06±0.02	0.06±0.02
24	Polar temporal sulcus right	curvature	0.20±0.08	0.19±0.06
25	Posterior inferior temporal sulcus	curvature ratio	1.40±0.76	1.21±0.67
26	Intermediate precentral sulcus	surface area ratio	0.98±0.68	0.92±0.63
27	Posterior lateral fissure left	surface area	3093.19±563.32	3180.43±559.75
28	Collateral fissure right	surface area	1198.95±529.62	1396.36±463.40
29	Polar temporal sulcus right	surface area	326.65±164.55	371.70±137.46
30	Rhinal sulcus	curvature ratio	1.19±1.39	0.95±0.59
31	Superior frontal sulcus left	surface area	1768.61±648.59	1852.34±660.76
32	Superior precentral sulcus right	volume	191.85±107.98	221.87±117.69
33	Parieto-occipital fissure right	curvature	0.08±0.04	0.08±0.04

rate against the false positive rate (Figure 4). The ROC-AUC with the selected feature combination were 84%, based on 33 features (Table 2) from 24 sulci (Figure 5).

Discussion

The main objective of this paper was to investigate the sulcal morphology (mean curvature, surface area, volume) to evaluate the pattern recognition classification ability to distinguish between CN and AD subjects. Previous studies based solely on sulcal morphology have not, to the best of our knowledge, been able to achieve the same levels of specificity and sensitivity. Our results show that sulcal morphology, when based on specific features, could be used as a valuable biomarker. The contribution of this study is that it successfully investigated a classifier combination of sulcal mean curvature, surface area and volume, while

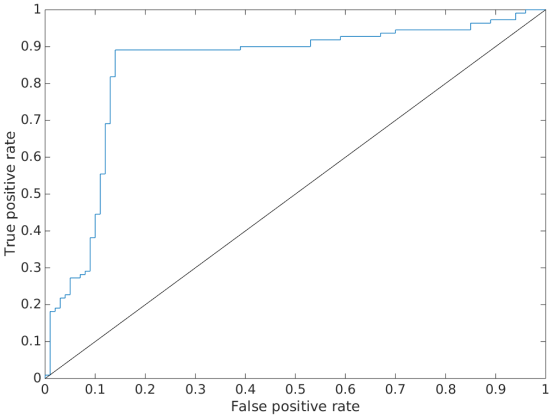

Fig. 4. ROC-curve for the AD/CN classification. The diagonal representing the random guess.

earlier studies focused on individual analysis of sulcal length, depth or width. The SVM classification of this study was based on a total of 33 features from 24 sulci (Figure 5). Several other classification methods have been proposed in literature to automatically distinguish between AD/MCI and cognitively normal controls [16,17]; a majority of them are multimodal. A study by [18], which combined three modalities of biomarkers (MRI, FDG-PET, and CSF), achieved a classification accuracy of 93.2%, 93% sensitivity, and 93.3% specificity, when combining all three modalities. However, a lower accuracy of 86.5% was achieved with the best individual modality, PET. With MRI alone, the specificity obtained was 86.3%, sensitivity 86% and accuracy 86.2%. Our study achieved a specificity of 89%, sensitivity of 86% and accuracy of 87% based on sulcal morphology from T1-weighted MRI, which therefore demonstrates promising results in the classification of AD and CN subjects.

The significance of our results facilitates further sulcal morphology studies in a combination with other biomarkers in order to improve early AD diagnosis. Most of sulcal morphology research on AD investigates very specific sulci, such as the central sulcus [19,20], or a combination of a few major, large sulci, since they are present in all individuals, they are relatively easy to identify and extract, and are located on different cerebral lobes [5,6]. Our approach involved the initial extraction of all cortical sulci. The subsequent feature extraction and selection excluded some sulci, which were incompletely extracted. Nonetheless, a large set of cortical sulci was studied (Figure 5). They varied in size and shape, and were located on different cerebral lobes, thus allowing us to investigate potential changes in sulcal morphology across the entire brain. The SVM classification in our study was based on 33 features (Table 2) from 24 sulci. The extracted sulci, which showed morphologic changes, were from the areas that are proved to be affected by AD atrophy. The Collateral fissure is located near the hippocampal

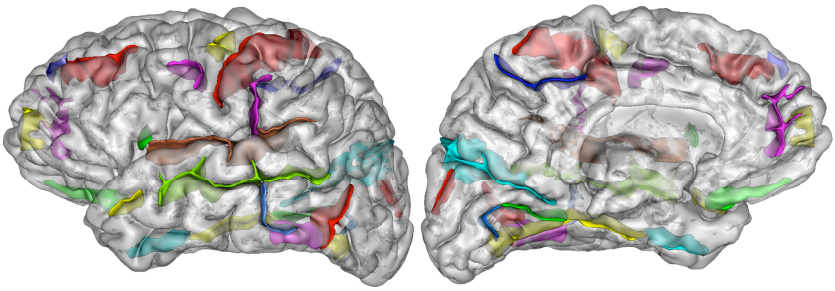

Fig. 5. The sagittal view of the selected 24 sulci

region where AD atrophy has been indicated [21,22]. Seven sulci (collateral fissure, rhinal sulcus, posterior inferior temporal sulcus, polar temporal sulcus, superior temporal sulcus, anterior inferior temporal sulcus, and the anterior terminal ascending branch of the superior temporal sulcus) are located in the medial temporal lobe, where AD atrophy also has been found [23–25]. The Callosomarginal posterior fissure and superior postcentral intraparietal superior sulcus are located in the parietal lobe, where morphological changes in AD have also been observed [22,24,26].

There are some potential limitations that should be addressed. BrainVISA toolbox is a commonly used sulcal identification and extraction pipeline. While the software is very efficient in automatically labeling and extracting the sulci, it is often advisable to address the data quality issue of the program. The majority of studies visually inspect the sulci after extraction to remove errors. This proves to be impossible with an immense set of subjects (n = 210) and sulci per subject (n = 120), since the initial extraction procedure resulted in a total of 25200 individual sulci. To asses the pipeline's performance and evaluate the quality of sulcal extraction, we performed an additional examination of a small subset of sulci (n=62) from 31 CN and 31 AD subjects. In this dataset, some of the extracted sulci (n=10) contained missing fragments, possibly due to lower quality of some MRI data, or an error in sulcal identification and labelling. It must be mentioned that this may have an impact on the calculated features. However, while it is possible that BrainVISA pipeline introduces a bias to the data, it still provides high classification results.

References

1. Prince, M., Bryce, R., Albanese, E., et al.: The global prevalence of dementia: a systematic review and metaanalysis. Alzheimer's & Dementia **9**(1), 63–75 (2013)
2. Uzun, S., Kozumplik, O., Folnegović-Šmalc, V.: Alzheimer's dementia: current data review. Collegium antropologicum **35**(4), 1333–1337 (2011)
3. Sonkusare, S.K., Kaul, C.L., Ramarao, P.: Dementia of Alzheimer's disease and other neurodegenerative disorders-memantine, a new hope. Pharmacological Research **51**(1), 1–17 (2005)

4. Brookmeyer, R., Johnson, E., Ziegler-Graham, K., Arrighi, H.M.: Forecasting the global burden of Alzheimer's disease. Alzheimer's & dementia **3**(3), 186–191 (2007)
5. Im, K., Lee, J.-M., Seo, S.W., et al.: Sulcal morphology changes and their relationship with cortical thickness and gyral white matter volume in mild cognitive impairment and alzheimer's disease. Neuroimage **43**(1), 103–113 (2008)
6. Liu, T., Sachdev, P.S., Lipnicki, D.M., et al.: Longitudinal changes in sulcal morphology associated with late-life aging and mci. NeuroImage **74**, 337–342 (2013)
7. Shokouhi, M., Williams, J.H.G., Waiter, G.D., Condon, B.: Changes in the sulcal size associated with autism spectrum disorder revealed by sulcal morphometry. Autism Research **5**(4), 245–252 (2012)
8. Cachia, A., Paillère-Martinot, M.-L., Galinowski, A., et al.: Cortical folding abnormalities in schizophrenia patients with resistant auditory hallucinations. Neuroimage **39**(3), 927–935 (2008)
9. Thompson, P.M., Hayashi, K.M., De Zubicaray, G., et al.: Dynamics of gray matter loss in Alzheimer's disease. The Journal of Neuroscience **23**(3), 994–1005 (2003)
10. Braak, H., Braak, E.: Neuropathological stageing of Alzheimer-related changes. Acta Neuropathologica **82**(4), 239–259 (1991)
11. Kochunov, P., Thompson, P.M., Coyle, T.R., et al.: Relationship among neuroimaging indices of cerebral health during normal aging. Human Brain Mapping **29**(1), 36–45 (2008)
12. Liu, T., Wen, W., Zhu, W., et al.: The relationship between cortical sulcal variability and cognitive performance in the elderly. Neuroimage **56**(3), 865–873 (2011)
13. Shen, D., Wee, C.-Y., Yap, P.-T.: Prediction of Alzheimer's disease and mild cognitive impairment using cortical morphological patterns. Wiley Periodicals Inc. (2012)
14. Stanojevic, M.: Proof of the hero's formula according to R. Boscovich. Mathematical Communications **2**, 83–88
15. Garde, A., Voss, A., Caminal, P., Benito, S., Giraldo, B.F.: Svm-based feature selection to optimize sensitivity-specificity balance applied to weaning. Computers in Biology and Medicine **43**(5), 533–540 (2013)
16. Davatzikos, C., Fan, Y., Wu, X., Shen, D., Resnick, S.M.: Detection of prodromal Alzheimer's disease via pattern classification of magnetic resonance imaging. Neurobiology of Aging **29**(4), 514–523 (2008)
17. Misra, C., Fan, Y., Davatzikos, C.: Baseline and longitudinal patterns of brain atrophy in MCI patients, and their use in prediction of short-term conversion to AD: results from ADNI. Neuroimage **44**(4), 1415–1422 (2009)
18. Zhang, D., Wang, Y., Zhou, L., Yuan, H., Shen, D.: Multimodal classification of Alzheimer's disease and mild cognitive impairment. Neuroimage **55**(3), 856–867 (2011)
19. Li, S., Xia, M., Fang, P., et al.: Age-related changes in the surface morphology of the central sulcus. Neuroimage **58**(2), 381–390 (2011)
20. McKay, D.R., Kochunov, P., Cykowski, M.D., et al.: Sulcal depth-position profile is a genetically mediated neuroscientific trait: description and characterization in the central sulcus. The Journal of Neuroscience **33**(39), 15618–15625 (2013)
21. Morra J.H., Tu, Z., Apostolova, L.G., et al.: Automated mapping of hippocampal atrophy in 1-year repeat mri data from 490 subjects with Alzheimer's disease, mild cognitive impairment, and elderly controls
22. Farias, S.T., Jagust, W.J.: Neuroimaging in non-alzheimer dementias. Clinical Neuroscience Research **3**, 383–395 (2004)

23. Ishii, K., Kawachi, T., Sasaki, H., et al.: Voxel-based morphometric comparison between early- and late-onset mild alzheimer's disease and assessment of diagnostic performance of z score images
24. Frisoni, G.B., Pievani, M., Testa, C., et al.: The topography of grey matter involvement in early and late onset Alzheimer's disease
25. Hamelin, L., de Souza, L.C., Corlier, F., et al.: Improved accuracy of the diagnosis of early Alzheimer's disease using combined measures of hippocampal volume and sulcal morphology (p4. 016). Neurology **82**(10 Supplement), P4–016 (2014)
26. Sabuncu, M.R., Desikan, R.S., Sepulcre, J., et al.: The dynamics of cortical and hippocampal atrophy in Alzheimer disease